JOURNAL OF MATERIALS SCIENCE 33 (1998) 1119–1128

Damage performance of particles filled quasi-isotropic glass–fibre reinforced polyester resin composites

V. K. SRIVASTAVA, P. J. HOGG
Department of Materials, Queen Mary And Westfield College, University of London, Mile End Road, London, E1 4NS, UK
E-mail: vijayks@banaras.ernet.in

The purpose of this work was to determine the toughening mechanisms in interlayered quasi-isotropic glass–fibre reinforced polyester resin (GFRP) composites. Particles of polyethylene and aluminium tri-hydrate, $Al(OH)_3$, were mixed with the polyester resin prior to laminating with woven E-glass-fibre cloth. Mode-I, mode-II, and impact tests were performed to determine critical strain energy-release rates (G_{Ic} and G_{IIc}), absorbed energy and residual compressive strength for the laminates with and without particulate additions. Mode-I and mode-II delamination toughness were characterized using double cantilever beam (DCB) and end-notched flexure (ENF) specimens, respectively, and the delaminated surfaces of specimens were examined using scanning electron microscopy (SEM) to investigate the interlaminar morphology after fracture. The results indicate that the interlaminar toughness (G_{Ic} and G_{IIc}), absorbed energy and residual compressive strength values of the GFRP composite increases with increase of particle content. The improved behaviour of particle containing GFRP is linked to stress-concentration induced plastic deformation and crack bridging. Polyethylene particles increase the toughness of the matrix material, which results in composites with higher values of mode-I, mode-II and impact than the composites with aluminium tri-hydrate particles. © *1998 Chapman & Hall*

1. Introduction

Laminates based on glass fabrics are used in a variety of structural applications for reinforcement. Fibre-reinforced polymer composites (FRP) often consist of two major components: an inorganic phase, such as glass fibre, and an organic polymer matrix, such as an epoxy resin. The physical properties of composite materials are determined by the properties of their components and composite structure. Although it is often difficult to separate the contribution of each to the composite behaviour. Fibre-reinforced polymeric composite laminates have traditionally suffered poor resistance to interlaminar fracture caused during out-of-plane impact. During a typical low-velocity impact event which, for example, might be caused by a bird strike or a dropped tool, the composite panel is loaded dynamically in flexure. This loading condition gives rise to significant shear stress in the material beneath the impact site, causing the generation of microcracks within the plies [1–3]. As these microcracks grow into the resin-rich interlaminar region between crossed-plies, they can be redirected into the interply as delaminations if the impact energy is high enough. The delamination caused during the fracture event severely reduces the residual compressive strength of most laminated composites [4–5].

The resistance to crack propagation is usually characterized by toughness i.e. the energy dissipated on creation of new surfaces. Interlaminar toughness of reinforced composites depends on several factors. For example, composite toughness increases with increase in toughness of the matrix [6–7], with an increase of the matrix thickness in the space between neighbouring fibres and with decrease in fibre content [8–9]. The toughness of epoxy polymers has been shown to be associated with the size of the plastic zone that appears in the tip of growing cracks in composites. The size of this plastic zone is restricted by the space between the fibres, and is therefore lower in comparison with that in the neat resin [3]. For the same reason, large increases in neat resin toughness have only a modest effect on interlaminar toughness. In unidirectional carbon and glass fibre reinforced composites with epoxy matrices, typical values of interlaminar mode-I toughness G_{Ic} are in the range 200–400 J m^{-2}. Modification of the epoxy matrix with rubber particles leads to improvement in G_{Ic} up to approximately 800–1000 J m^{-2}. For composites reinforced by woven glass fibres, typical values of the mode-I toughness are in the range 800–1000 J m^{-2}, even if the matrix has not modified by rubber [6]. The plastic yield zone in fabric-reinforced composites is determined by the space between the fabric layers, which is much larger than that between adjacent fibres in the layers, and hence higher G_{Ic} and G_{IIc} are measured.

Work on particle filled composites indicates that the toughening mechanisms of virgin materials are improved marginally [10]. It is believed that the particles act to bridge the microcracks which form in the interply during fracture. Such bridging may absorb substantial energy in the subsequent deformation of the particles, thus limiting delamination [11]. A composites resistance to delamination during impact has been found to correlate well with mode-II fracture energy release rate (G_{IIc}) [11–12]. This correlation has been attributed to the shear, or mode-II loading condition under which delaminations grow during impact. Several researchers have studied the effect of interply thickness and resin ductility on G_{IIc} [3, 10, 13]. In general, increases in interply thickness and resin ductility have been found to increase the mode-II fracture toughness of the composites.

The focus of the present work was to determine the effect of particles on the mode-I, mode-II interlaminar toughness, post-impact residual compressive strength and absorbed energy during impact of quasi-isotropic glass–fibre reinforced polyester resin composites. The primary variables for this study were (1) the type of particles (polyethylene and aluminium tri-hydrate), (2) the concentration of the particles in the resin and (3) the variation in pre-crack length. In addition to measuring the damage tolerance of each system, the modes of deformation and failure were examined using scanning electron microscopy, in order to determine the mechanism of toughening of each system.

2. Materials

The reinforcing material used was an E-glass fibre quadriaxial fabric (weight 610 g m^{-2} and dry thickness 0.55 mm). The matrix system was an epoxy–vinylester resin (Derakane 411–45, Accelerator-E, 2% of the resin and Catalyst-M, 3% of the resin) supplied by Dow Europe. Polyethylene (40 μm) and aluminium tri-hydrate, $Al(OH)_3$, (10 μm) were used as filler materials.

Laminates, nominally 2.5 mm thick were prepared by hand lay-up at room temperature. The particulate materials, ranging from 5 to 15% by weight of the matrix, were added to the polyester resin before it was applied to the glass fibre cloth, care was taken to avoid agglomeration of the particles. In the following discussion, these materials will be referred to, for convenience as Pl-GFRP (polyethylene-filled) and Al-GFRP (Aluminium tri-hydrate-filled). During fabrication of the laminate, the vinylester resin flowed from the blended resin into the fabric; however, the particles, were effectively filtered by the fabric and largely left in the interply regions as shown in Fig. 1. Teflon film (0.5 mm thick) was also inserted on the mid-plane at one edge of some laminates to provide a starter notch for interlaminar toughness test. The laminates were post-cured at 85 °C for 12 h, following the manufacturer's recommendations. The final fibre-volume fraction of all laminates was about 0.40 based on weight of materials used. Specimens were cut with a water cooled diamond cutting wheel and dried for 1 h at 100 °C.

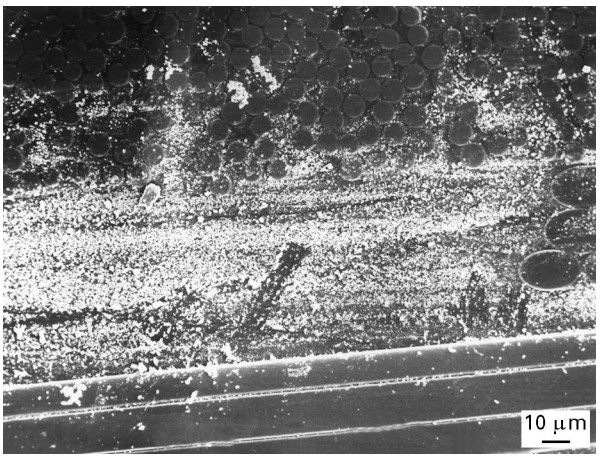

Figure 1 SEM micrographs shows the distribution of particles (appears in white colour) inside the composites.

3. Testing procedure

3.1. Interlaminar toughness tests

The resistance to delamination growth can be characterized by the strain energy release rate (G), where the critical energy release rate (G_c) is used as a measure of the interlaminar toughness. Several different analytical approaches have been utilized in determining values of G_{Ic} and G_{IIc}.

In the present work, the toughness will be estimated by using mode-I; double cantilever beam (DCB) and mode-II; end notched flexure (ENF) tests. The test specimens for DCB and ENF were 160 mm long, 21 mm wide and 2.5 mm thick. The starter notch length was 40 mm.

3.1.1. Mode-I testing

For mode-I testing, steel piano hinges were glued onto the surface of the beam at the notch for application of the load to the specimen during testing. The sides of the specimen were painted white in order to permit visual crack-tip location. The test specimens were loaded in an Instron testing machine at a crosshead speed of 10 mm min^{-1}. The experimental fracture data were recorded in the form of the complete load/displacement curve for the sample-1 as shown in Fig. 2a and b.

From load, displacement and crack length, the strain energy release rate (G_{Ic}) may be calculated by using the general formula from linear elastic fracture mechanics (LEFM) [14]

$$G_{Ic} = (P_C^2/2W)\,dC/da \quad (1)$$

where P_C is the critical load at which the crack grows, W is the width of the specimens, C is the compliance and a the initial crack length.

Compliance, C, may be obtained experimentally, as shown in Fig. 3, by using the relationship

$$C = \delta_C/P_C \quad (2)$$

where δ_C and P_C are the critical displacement and load.

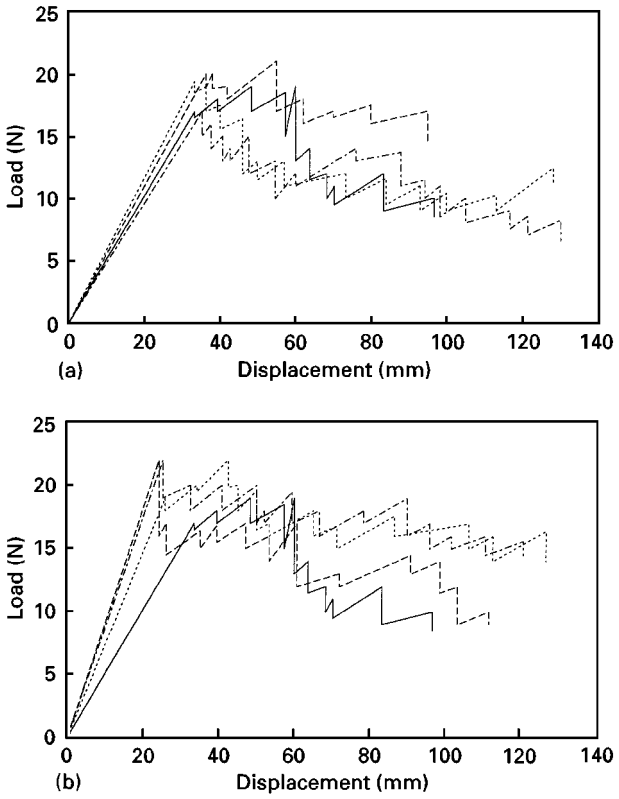

Figure 2 Load–displacement diagrams of DCB test: (a) GFRP and Al-GFRP composites and (b) Pl-GFRP composites (——) GFRP; (– – – –) 5% Al-GFRP; (- - - - - -) 10% Al-GFRP; (– – – –) 15% AI-GFRP.

Also, the relationship between compliance and crack length may be obtained using simple beam theory, and can be written as

$$C = Aa^3 \tag{3}$$

where A is an experimentally determined parameter, which is geometry and material dependent.

After differentiating Equation 3 and substitution into Equations 1 and 2 we have

$$G_{Ic} = 3P_C\delta_C/2Wa \tag{4}$$

However, this relationship is only valid for the ideal conditions assumed in the beam theory; corrections are necessary for large displacements, shear deformation and rotation at the crack-tip. Some of these effects can be taken into account by correcting the crack length, a. The crack length correction, Δ, for all specimens may be found by plotting the cube root of compliance against the crack length (Fig. 4), as listed in Table I. This gives an approximately straight line which intersects the crack length axis at Δ. The critical strain-energy release rate now becomes

$$G_{Ic} = 3P_C\delta_C/2W(a + \Delta) \tag{5}$$

which will be referred to as the corrected LEFM formula.

A different approach for finding the critical strain energy release rate is the area method [14]. The energy, ΔU, dissipated in the specimen during crack propagation is measured directly from the loading and unloading load/displacement curves in a DCB test, and the increment, Δa, of new crack length. The formula for calculation of, G_{Ic}, is

$$G_{Ic} = \Delta U/W\Delta a \tag{6}$$

By this method an average toughness value during propagation is established for each loading–unloading cycle. An average G_{Ic} value may be obtained from a series of loading and unloading curves.

3.1.2. Mode-II Testing

The end-notch flexure (ENF) fracture test was to measure mode-II delamination resistance. This is a three-point bend test in which the specimen contains

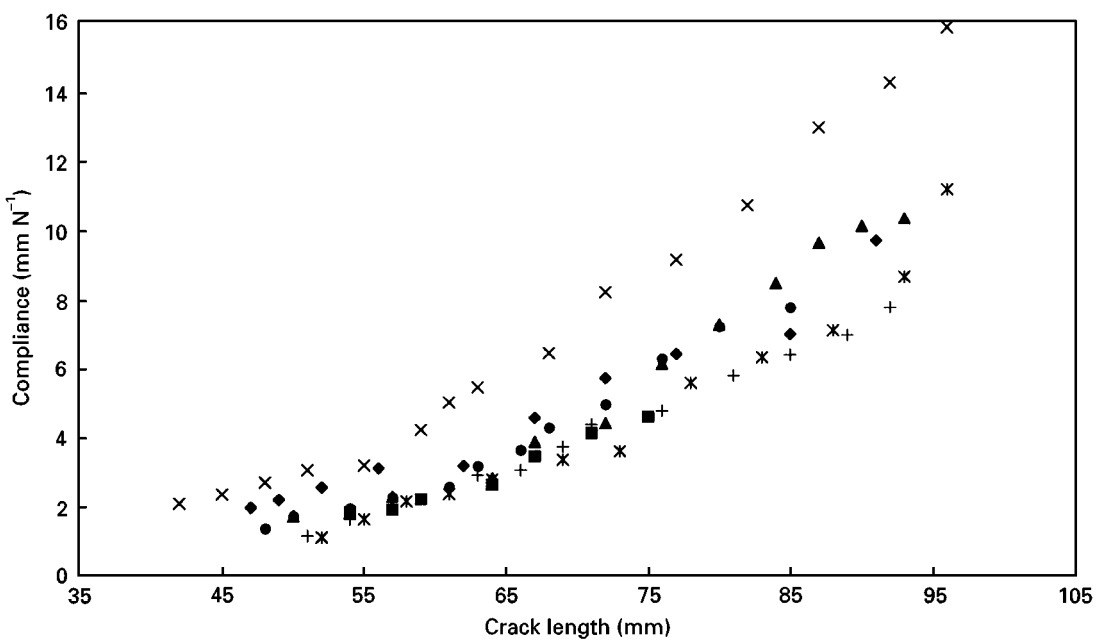

Figure 3 Typical compliance calibration curves for filled and unfilled GFRP composites (◆) GFRP; (■) 5% Al-GFRP; (▲) 10% Al-GFRP; (×) 15% Al-GFRP; (∗) 5% Pl-GFRP; (●) 10% Pl-GFRP; (+) 15% Pl-GFRP.

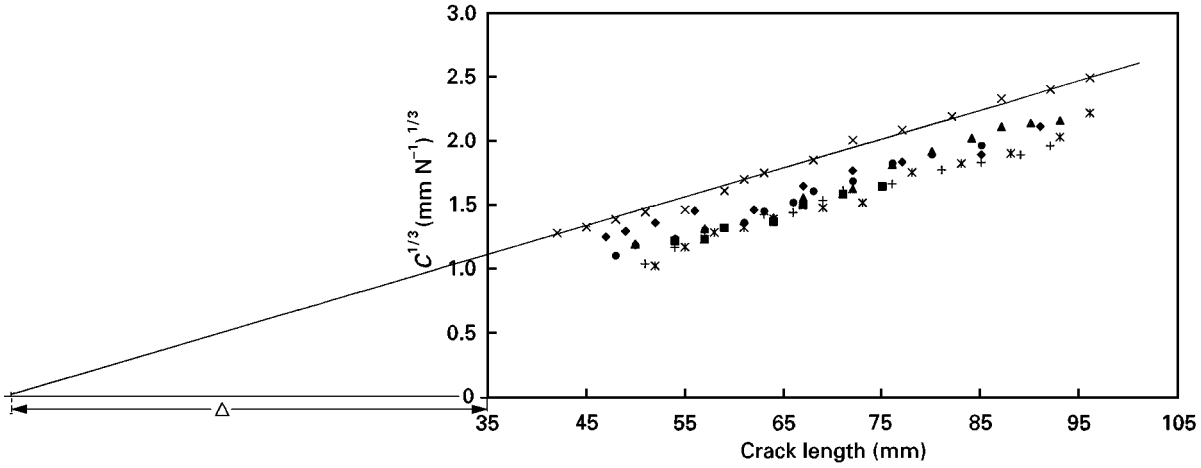

Figure 4 $C^{1/3}$ plotted against crack length, for determining the value of correction factor. (◆) GFRP; (■) 5% Al-GFRP; (▲) 10% Al-GFRP; (×) 15% Al-GFRP; (✳) 5% Pl-GFRP; (●) 10% Pl-GFRP; (+) 15% Pl-GFRP.

TABLE I Correction factor, Δ, may be obtained from cube root of the compliance and crack length curves for all materials

Materials	Correction factor, Δ (mm)
GFRP	35.48
5% Al-GFRP	33.15
10% Al-GFRP	37.18
15% Al-GFRP	38.50
5% Pl-GFRP	32.0
10% Pl-GFRP	32.68
15%Pl-GFRP	30.57

a precrack. The specimen is placed in such a way that the crack tip is midway between the loading roller and the outer support. The load is applied as controlled displacement (displacement rate 20 mm min^{-1}) and the crack growth is unstable in all cases. During the experiment the curve of load against centre-line deflection was recorded (see Fig. 10a and b). When the crack starts growing, a sudden load drop is observed and the test is stopped. The maximum recorded load and corresponding displacement is used in the data reduction process. Simple beam theory allows the calculation of the compliance, C, and upon inserting in Equation 1, the critical strain energy release rate can be calculated as [15]

$$G_{IIc} = 9a^2 P_C \delta_C / 2W(2L^3 + 3a^3) \quad (7)$$

where L is the half-span and δ_C is the critical displacement.

3.2. Impact test

Characterization of mechanical properties as a function of processing conditions was also carried out using impact tests.

For the purpose of low-energy impact testing a drop weight impact machine was used. This type of test ensures that the energy incident upon the specimen is insufficient to cause through penetration but sufficient to cause measurable damage and hence differs from high energy impact tests which use an incident energy in excess of that needed to form permanent damage [4, 16]. Low-velocity impact tests were conducted on clamped rectangular plates (60 × 60 × 2.5 mm) using an instrumented drop-weight test rig with a hemispherical impactor diameter of 20 mm. A clamping plate with a hole of diameter of 40 mm was used in order to obtain reproducible impact responses for specimens with slightly different widths. The impacting mass (2.406 kg) and height of impact (0.70 m), which gives an incident energy of 16.5 J were used for all the specimens. The force variation under impact is recorded by a CEAST advanced fractoscope system MK3 data recorder. This recorder then transfers the data to a computer on which the displacement, energy absorbed and velocity incident on the specimen can be calculated at any time, t. After impact, each specimen was visually inspected for surface damage. The residual compressive strength of impacted specimens were measured through the compression-after-impact (CAI) test. For the compression part of the test, a special jig was used to prevent buckling [17]. The fracture load was recorded on a Schenck Trebel machine (Instron) with a 100 kN load cell at a loading rate of 5 mm min^{-1}.

4. Results

4.1. Fracture toughness mode-I

The load–displacement curves of DCB samples of the plain GFRP and the filled composites are shown in Fig. 2a and b. The linear and non-linear elastic and non-linear inelastic response were observed and slow incremental crack growth initiates at the highest load level. The non-linear elastic region is due to large displacements; this is a result of the low flexural rigidity of the test coupons. From the loading and unloading curves, the compliance versus crack length and cube root of the compliance versus crack length are obtained, as shown in Figs 3 and 4. The results show that for all laminates the compliance increased with increasing crack length. This relationship, $C = Aa^3$, is used for the determination of the mode-I strain energy release rate, (G_{Ic}).

The critical strain energy release rate, G_{Ic}, was calculated using compliance measurements and area

under the load–deflection curve at various points along the experimental force deflection curves.

The individual data points calculated in this way exhibited some degree of variation both within a specimen and between different specimens. In most cases the different material types could be considered to exhibit some form of *R*-curve behaviour with G_{Ic} rising as the crack length increased.

There was little consistency in behaviour across the various groups of specimens and between data calculated using both compliance and area methods. Some materials exhibited *R*-curve behaviour with the compliance measurements but did not show any consistent rise in G_{Ic} when calculated using the area method e.g. the unmodified GFRP. Some materials revealed a levelling off of G_{Ic} values after a certain length of crack growth, while others exhibited a steadily increasing G_{Ic} in which the toughness increased in a linear fashion with crack length. Again, different trends could be observed between compliance and area methods within the data for a given material type but there was no consistent difference between the results from each type of measurement over all material types.

Data points calculated using the compliance and area methods were however reasonably similar for all groups of specimens. In order to compare the values of G_{Ic} derived from the experimental data, a representative value was chosen as the toughness where the G_{Ic} appeared to become independent of crack length. In most cases where this behaviour was observed the crack length was of the order of 90 mm. Where the value did not become independent of crack length then the G_{Ic} value was taken as the maximum recorded during the experiment which again usually corresponded to a crack length of the order of 90 mm. The values selected for each material type are indicated at point A on the G_{Ic} versus crack length in Figs 5a to g and 6a to g. Specimen-to-specimen scatter shown in Figs 5a to g and 6 a to g are thought to be due to splitting in the vicinity of the crack tip. The initial value was calculated from the load at which initial-crack propagation from the insert occurs. After an increment of crack growth of about 4 mm, the specimens were unloaded and then re-loaded to obtain a second G_{Ic} value corresponding to another 4 mm increment of crack growth ahead of the insert. This method is a means of avoiding problems arising from the resin-rich region usually associated with the presence of the insert [10]. At the smaller crack lengths, G_{Ic} increases with crack length and levels off after the crack has grown about 15 mm. If the crack propagates further, then G_{Ic} increases again. Because the process of fibre bridging and microcrack bridging (because of particles) involves peeling the fibres from the matrix and fracture of the fibres as the separation of the arm increases, a part of the energy is dissipated in the bridged zone before reaching the crack tip as can be identified from Fig. 7a and b. It is clear that the nested microcrack bridging occurred in front of the crack tip. Therefore, a higher load or energy is required to produce the critical condition at the crack tip which causes an increase in fracture toughness. This rising *R*-curve is commonly observed in these tests and is attributed to the growth of a zone of nested fibres bridging and microcrack bridging the crack faces [7–9].

Representative G_{Ic} values for each specimen data set are plotted against weight of filler in Fig. 8. The data indicates that particle content has little effect on the aluminium tri-hydride-filled composites over the range investigated. The polyethylene in contrast does appear to toughen the composite, particularly on the basis of toughness calculated using the compliance methods. However, it would appear that a maximum value is reached at about the 10% filler level after which the additional filler causes the toughness to fall.

Scanning electron microscopy (SEM) micrographs of the fractured surface of the interlayered system are shown in Fig. 9a and b. The damage features indicate that microcracking occurs in the matrix around the particulates filler. These microcracks interact with the surrounding particles, growing through and around them.

4.2. Fracture toughness mode-II

The load–displacement curves from the ENF test are shown in Fig. 10a and b. In most cases, two basic regions appeared in the load–displacement curves, these corresponding to linear and non-linear regions. The large displacements and rotations can give rise to a non-linear elastic response, which will be followed by damage initiation.

Model-II, toughness, G_{IIc}, values were calculated from the critical load and displacement values from each curve (Table II) by using Equation 7, and the average values are shown plotted against filler content in Fig. 11. The results indicate that the mode-II, toughness, G_{IIc}, increases with additions of both polyethylene and aluminium tri-hydrate particles. A maximum is observed in the region of 10% additions, for both types of particles. Polyethylene additions again give higher G_{IIc} values than the aluminium tri-hydrate, perhaps because of their ability to yield, low modulus and adhesion between the filler and the matrix. Large numbers of shear cusps (hackles) were observed lying in the valleys as shown in Fig. 12a. It was observed that the fracture surface of the upper arm of the specimen contained fibres but hardly any fibres imprints (Fig. 12b), while the matching lower surface contained imprints but hardly any fibres (Fig. 12a). It is also noteworthy that the microcracks which initiate the hackles between the fibres in the non-interlayered brittle systems do not tend to continue to grow into the interply. Thus, in the interlayered systems, the microcracks which form at the ply–matrix interface during delamination will not tend to grow into the particle-rich interply region and will not interact directly with the particles. The particles, then, must first generate microcracks within the interply in order to provide any significant toughening in the more highly crosslinked systems. If the particles did not initiate microcracking in the matrix, they would not act in a crack-bridging capacity [3].

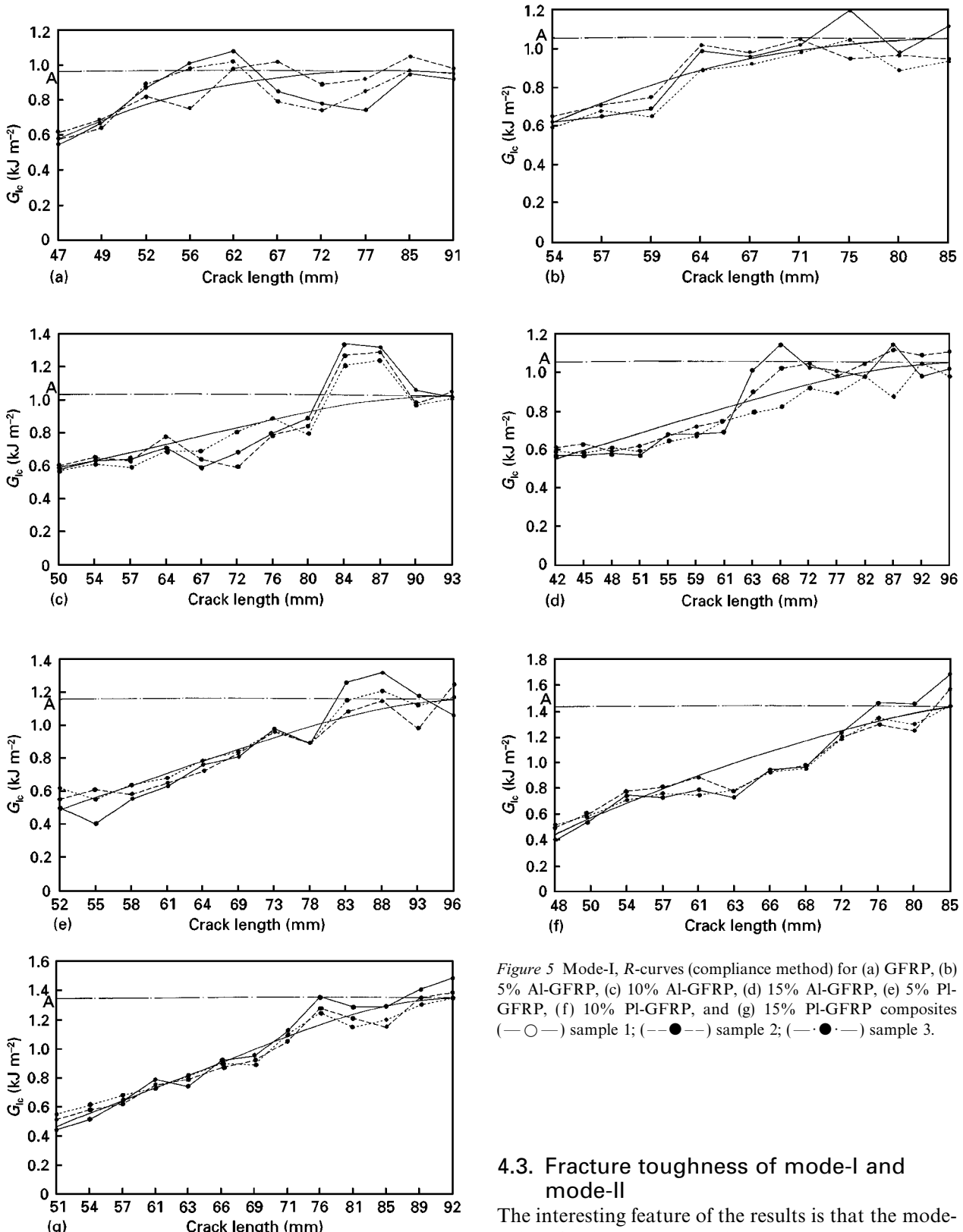

Figure 5 Mode-I, *R*-curves (compliance method) for (a) GFRP, (b) 5% Al-GFRP, (c) 10% Al-GFRP, (d) 15% Al-GFRP, (e) 5% Pl-GFRP, (f) 10% Pl-GFRP, and (g) 15% Pl-GFRP composites (— ○ —) sample 1; (– – ● – –) sample 2; (— · ● · —) sample 3.

The overall increase in mode-II toughness values indicate that several other mechanisms are responsible for the increase in energy absorption [7]. First, friction is an important energy absorbing mechanism. Secondly, the further development of hackles and large plastic zone in front of the crack tip due to presence of particles will absorb additional energy. The matrix is unable to deform freely because it is surrounded by particles and strong fibres. This may be partly a result of load transfer, which reduces the magnitude of the matrix stresses [13].

4.3. Fracture toughness of mode-I and mode-II

The interesting feature of the results is that the mode-II interlaminar toughness is up to about 50% higher than the mode-I toughness as listed in Table II. In the ENF test, mode-II crack propagation causes relative sliding of the crack surfaces. Friction between the crack surfaces may oppose the sliding and consequently increase the G_{IIc} values because the sliding of crack surfaces is arrested by the particles, as can be visualized by Fig. 12a and b. Mode-I and mode-II values are lower for aluminium tri-hydrate additions than for the polyethylene additions. This reveals that the polyethylene filler is more effective in toughening of GFRP composites.

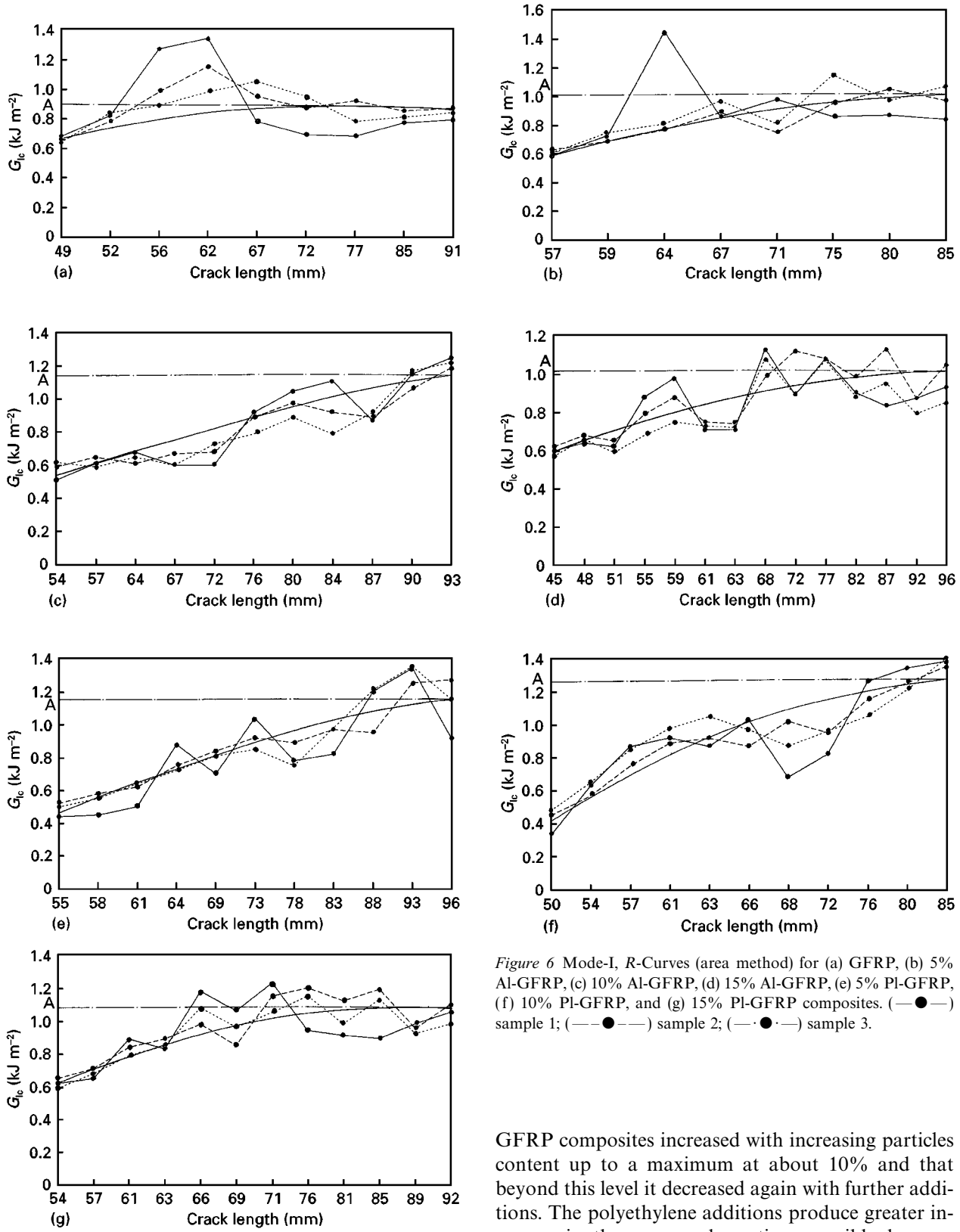

Figure 6 Mode-I, *R*-Curves (area method) for (a) GFRP, (b) 5% Al-GFRP, (c) 10% Al-GFRP, (d) 15% Al-GFRP, (e) 5% Pl-GFRP, (f) 10% Pl-GFRP, and (g) 15% Pl-GFRP composites. (—●—) sample 1; (——●——) sample 2; (—·●·—) sample 3.

4.4. Impact response

Impact damage for the materials tested can be classified as either indentations or cracks. In some cases besides the damage in the impacted plane, damage extended through the laminate thickness and broken fibres protruded from the back surface of the specimen. The impact results (Figs 13 and 14) show that the absorbed energy and residual compressive strength of GFRP composites increased with increasing particles content up to a maximum at about 10% and that beyond this level it decreased again with further additions. The polyethylene additions produce greater increases in the energy absorption, possibly because polyethylene particles increase G_{IIc} of the composites. Residual compressive strengths of the polyethylene-filled GFRP composites are independent of the level of filler content and are significantly higher than the neat resin composites, as can be seen from Fig. 14. In general, the residual compressive strength is directly related to the damage area exhibited by the materials [4–5]. Although the reduction of residual strength caused by the breakage of load-bearing fibres is serious, the existence of internal delamination is most deleterious for subsequent compressive loading.

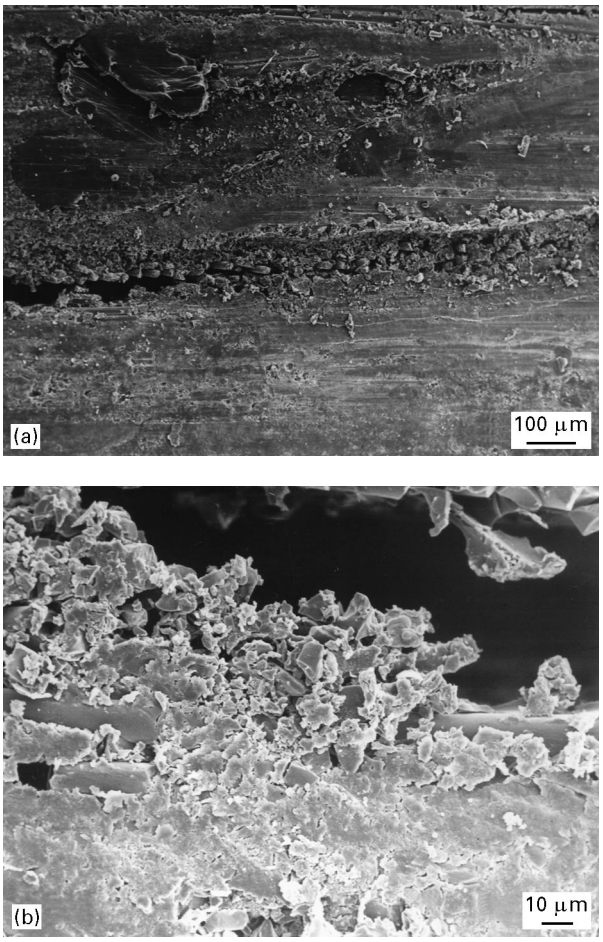

Figure 7 SEM micrograph showing that (a) the microcracking occurred along the path of crack and (b) nested microcrack bridging ahead of crack due to particles, under mode-I test.

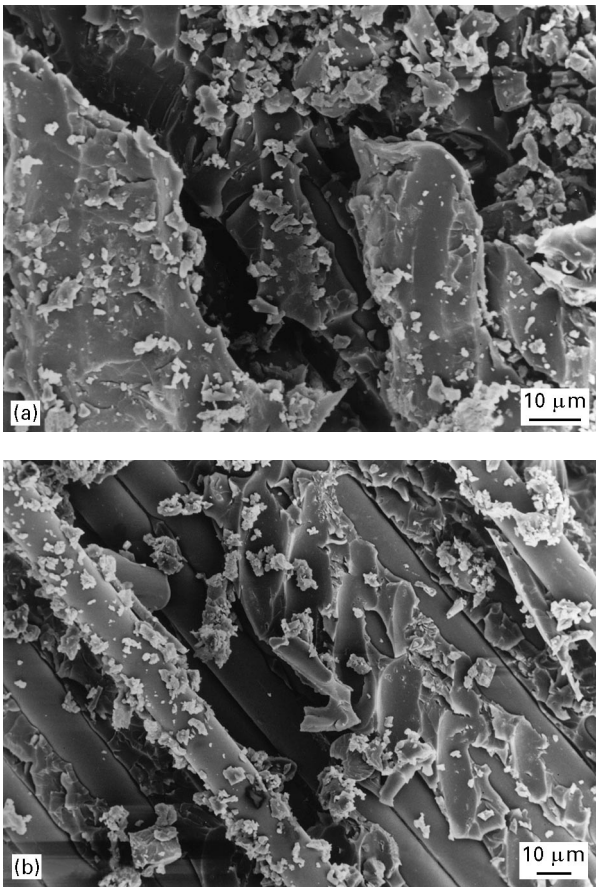

Figure 9 SEM micrograph showing that (a) the particles bridge the crack of the matrix system and (b) the particles settled around the fibres, as well as fibre debonded from the matrix.

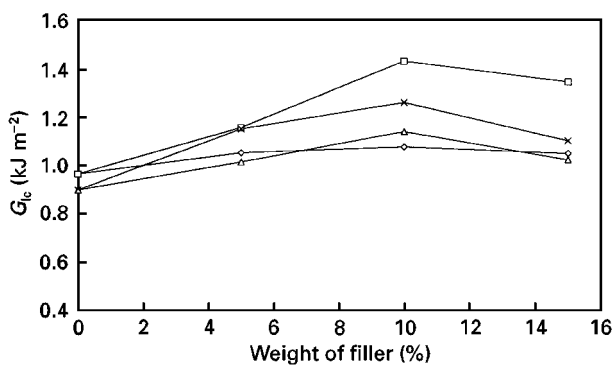

Figure 8 The effect of the filler content on interlaminar toughness, G_{Ic} (measured from Figs 5a to g and 6a to g) at point A for delamination growth in GFRP composites. (◇) Al-GFRP (compliance); (□) Pl-GFRP (compliance); (△) Al-GFRP (area); (×) Pl-GFRP (area).

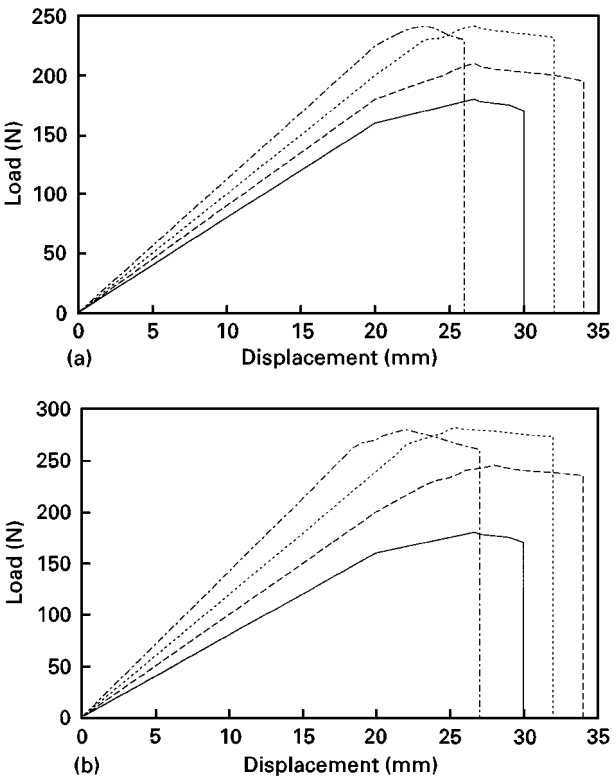

Figure 10 Load–displacement diagrams of ENF test: (a) GFRP and Al-GFRP composites and (b) Pl-GFRP composites. (——) GFRP; (– – – –) 5% Al-GFRP; (- - - - -) 10% Al-GFRP; (– – – – – –) 15% Al-GFRP.

5. Discussion

The introduction of particulate fillers in the interlaminar regions of glass fibre composites have been found to have little effect on the measured interlaminar G_{Ic} values for the composites. Some small improvement is measurable for the polyethylene additions. This suggests that the ability for particles to modify crack opening mechanisms and contribute to

TABLE II Mode-I and mode-II, interlaminar toughness, G_{Ic}, (measured at point A from Figs 4 and 5) and G_{IIc}, (average value) values for different materials

Materials	G_{Ic} (kJ m^{-2}) Compliance method	Area method	G_{IIc} (kJ m^{-2})
GFRP	0.966	0.899	1.246
5% Al-GFRP	1.053	1.014	1.454
10% Al-GFRP	1.036	1.139	1.675
15% Al-GFRP	1.047	1.02	1.46
5% Pl-GFRP	1.158	1.152	1.781
10% Pl-GFRP	1.43	1.26	1.854
15% Pl-GFRP	1.345	1.10	1.599

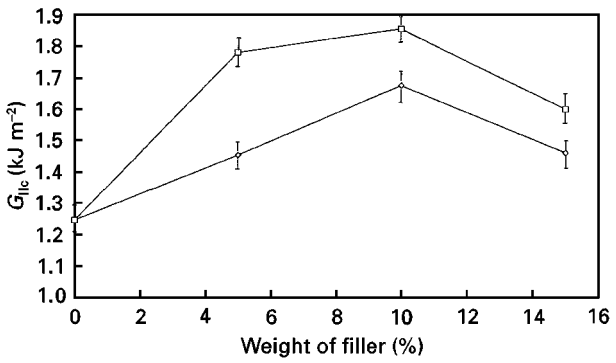

Figure 11 The effect of the filler content on the interlaminar toughness, G_{IIc}, for delamination growth in GFRP composites. (◇) Al-GFRP; (□) Pl-GFRP.

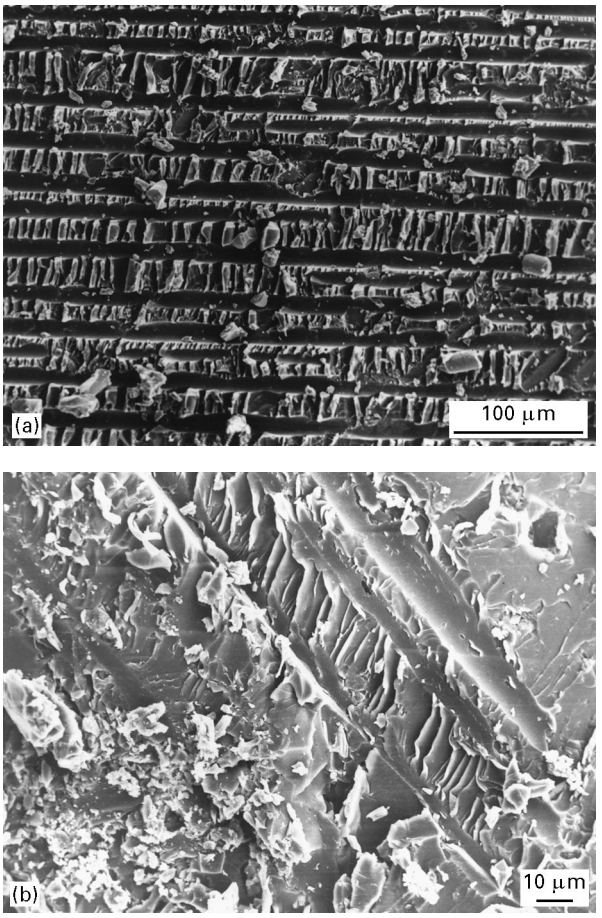

Figure 12 SEM micrograph showing (a) the large amount of hackles present on the surface and (b) the particles also bridge the crack path under mode-II test.

crack shielding via processes such as crack bridging and crack blunting (via branching and crack tip microcracking) are limited.

The effect of particles on mode-II crack sliding is, however, significant, particularly for the polyethylene-filled materials. The increased toughness in mode-II may be attributed to frictional effects in part and the necessity for a much larger surface area of crack to be generated as a result of crack roughening induced by the particle additions. The polyethylene particles have additional potential to absorb energy by plastically yielding, which is more likely to occur in mode-II than in a mode-I experiment.

It is generally accepted that impact damage in laminated composites is controlled by mode-II deformation and this view is consistent with the observation that particle additions increase the energy absorption in the laminates with the polyethylene-filled laminates exhibiting the greatest energy absorption.

The results obtained from compression after impact testing reveal some significant disparities between the two classes of filled composite. The ceramic filler reduces residual compression strength while the polymeric additions increase compression strength. Previous studies on a variety of fibre-reinforced composite systems have suggested that residual compression strength is not controlled by fracture mechanics parameters such as G_{Ic} or G_{IIc}, but rather by the area

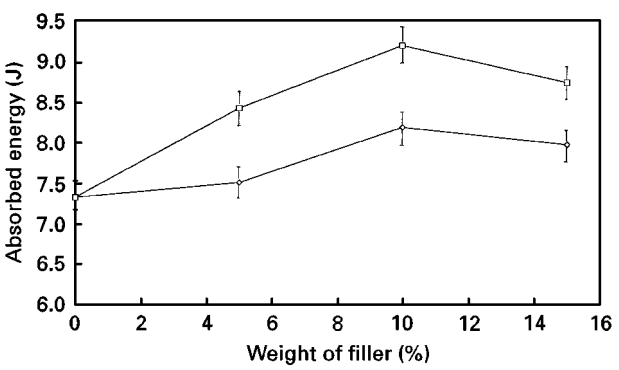

Figure 13 The effect of the filler content on the absorbed energy of the GFRP composites, for impact energy of 16.8 J. (◇) Al-GFRP; (□) Pl-GFRP.

of damage induced by the impact [17]. The damage zone acts as a soft region within a stiff laminate and acts to magnify stress locally. The addition of stiff ceramic filler would accentuate this effect by raising the effective stiffness of an undamaged laminate and creating a greater disparity between cracked (delaminated) areas and surrounding undamaged material. Conversely, the polyethylene additions would effectively reduce the stiffness of the laminate and minimize stiffness variations between damaged and undamaged zones, thereby reducing the stress magnification effects.

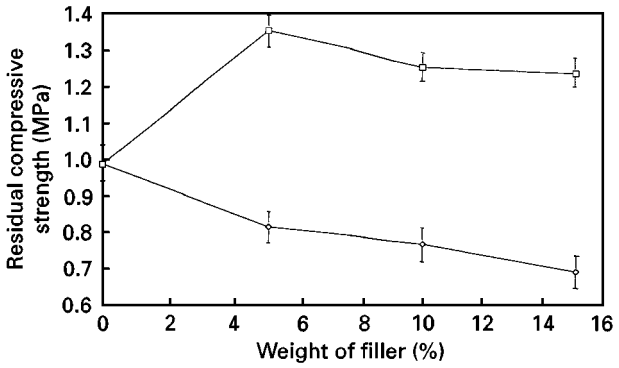

Figure 14 The effect of the filler content on the residual compressive strength of the GFRP composites, after a 16.8 J impact. (◇) Al-GFRP; (□) Pl-GFRP.

6. Conclusions

Based on the results presented here, the following conclusions may be drawn;

1. The addition of filler particles to glass-fibre reinforced composites will affect the mode-II interlaminar toughness significantly but, at the levels investigated result in only marginal changes in G_{Ic}.
2. The increase in mode-II toughness, G_{IIc} induced by ductile thermoplastic particles is greater than that induced by the addition of a hard ceramic particle.
3. The increase in mode-II toughness translates into improved energy absorption during impact.
4. The effect of ceramic and organic particle filler on the post impact compression strength are different and may be linked to the effective stiffening of the laminated introduced by each type of particle.

The conclusions identified from this work are restricted and can only apply to the two classes of particles studied. Variables that have not been studied and which may affect the results obtained and hence the trends observed include particle size effect, particle roughness and particle to matrix bonding.

Acknowledgements

This work was carried out at Department of Materials, Queen Mary & Westfield College, University of London, Mile End Road, London, El 4NS, UK, with the financial support of the British Council, London, UK. One of us (V. K. Srivastava) was the recipient of a Commonwealth Academic Staff Fellowship.

References

1. D. HULL and Y. SHI *Comp. Struct.* **23** (1993) 99.
2. S. P. JOSHI and C. T. SUN, *J. Comp. Mater.* **19** (1985) 51.
3. M. R. GOLEAU, Y. B. SHI, A. F. YEE, J. L. BERTRAM, H. J. SUE and P. C. YANG, *Comp. Sci. Technol.* **56** (1996) 1223.
4. G. ZHOU, *Comp. Struct.* **35** (1996) 171.
5. J. C. PRICHARD and P. J. HOGG, *Composites* **21** (1990) 503.
6. S. L. BAZHENOV, *ibid.* **26** (1995) 125.
7. N. SELA and O. ISHAI *ibid.* **20** (1989) 423.
8. H. J. SUE, J. E. JONES and E. I. GARCIA-MEITIN, *J. Mater. Sci.* **28** (1993) 6381.
9. T. W. H. WANG and F. D. BLUM *ibid.* **31** (1996) 5231.
10. V. K. SRIVASTAVA and B. HARRIS *ibid.* **29** (1994) 548.
11. J. MASTER, in Proceedings of the 6th International Conference on Composite Materials, vol. 3, (Elsevier, London, 1987) p. 396.
12. H. RECKER, *SAMPE J* **26** (1990) 73.
13. A. AKSOY and L. A. CARLSSON, *Engng Fract. Mech.* **39** (1991) 525.
14. J. M. WHITNEY, C. E. BROWNING and W. HOOGSTEDEN, *J. Reinf. Plast. Comp.* **1** (1982) 297.
15. A. J. RUSSELL and K. N. STREET, In "Delamination and debonding of materials," ASTM STP 876 (American Society for Testing and Materials, Philadelphia. PA, 1985) p. 349.
16. M. HOU, L. YE and Y. B. MAI, *J. Reinf. Plast. Comp.* **15** (1996) 1117.
17. F. J. GUILD, P. J. HOGG and J. C. PRICHARD, *Composites* **24** (1993) 333.

Received 16 June
and accepted 23 October 1997